

Ultrafast strong-field absorption in gapped graphene

S. Azar Oliaei Motlagh, Ahmal Jawad Zafar, Aranyo Mitra, Vadym Apalkov, and Mark I. Stockman
*Center for Nano-Optics (CeNO) and Department of Physics and Astronomy,
Georgia State University, Atlanta, Georgia 30303, USA*

(Dated: January 16, 2020)

We study theoretically the strong-field absorption of an ultrafast optical pulse by a gapped graphene monolayer. At low field amplitudes, the absorbance in the pristine graphene is equal to the universal value of 2.3 percent. Although the ultrafast optical absorption for low field amplitudes is independent of the polarization, linear or circular, of the applied optical pulse, for high field amplitudes, the absorption strongly depends on the pulse polarization. For a linearly polarized pulse, the optical absorbance is saturated at the value of ≈ 1.4 percent for the pulse's amplitude of ≥ 0.4 V/Å, but no such saturation is observed for a circularly polarized pulse. For the gapped graphene, the absorption of a linearly polarized pulse has a weak dependence on the bandgap, while for a circularly polarized pulse, the absorption is very sensitive to the bandgap.

I. INTRODUCTION

The progress in generation of ultrafast intense laser pulses provides powerful tools to observe the highly-nonlineer, strong-field phenomena in solids and expand the field of strong-field optics to both small time scales and high field intensities^{1–16}. Some of such strong-field phenomena are high harmonic generations, the ultrafast ionization, the nonlinear current generations, and the nonlinear optical absorption^{17–22}.

Graphene is a well known two dimensional (2D) solid made of a single layer of carbon atoms. It has a honeycomb crystal structure with two inequivalent sublattices, A and B ^{23,24}. The first Brillouin zone (BZ) of graphene is a hexagon and the corresponding energy dispersion is gapless at two Dirac points, K and K' , with the massless relativistic energy dispersion^{23–26}. The electron states at the Dirac points are chiral. They are characterized by nontrivial Berry phases $\pm\pi$, which are opposite at the K and K' points^{15,27–29}. The corresponding Berry curvature is non-zero only at the Dirac points, at which it has a δ -type singularity. For other 2D materials with the honeycomb crystal structure but with a finite bandgap, such as monolayers of transition metal dichalcogenides (TMDCs), the Berry curvature is non-zero within finite regions near the K and K' points with the maxima at these points^{15,29}. Thus, opening the bandgap in graphene-like materials broadens the Berry curvature in the K and K' valleys. Such broadening results in the effect of topological resonance³⁰, which occurs during ultrafast electron dynamics and is due to the compensation of the dynamic phase and the topological phase.

The gapped graphene has a broken inversion symmetry: the point symmetry group reduced from D_{6h} for graphene to D_{3h} . Consequently, a bandgap opens up at the K points. Previously, we have shown that, due to the existence of the bandgap, the topological resonance appears in strong fields. Consequently, a femtosecond intense optical pulse generates a large valley polarization³⁰, which is not related to the electron spin and the spin-orbit coupling (SOC).

Also, in the gapped graphene, in addition to the field-driven longitudinal current, there is a transverse current in the direction normal to the the applied field³¹. This transverse current is also due to breaking of the inversion symmetry; consequently, it strongly depends on the bandgap.

One of the important characteristics of the interaction of an optical pulse with solids is the absorption coefficient. For the pristine graphene, in the linear regime, approximately 2.3 percent of the incident light energy is absorbed. In a sharp contrast, the nonlinear absorption, which was measured for a 80-fs optical pulse, showed a saturable behavior^{20–22}. For such a long pulse, the electron dynamics in the field of the pulse is incoherent, and scattering and relaxation processes are important. Here, we study the absorption by the gapped graphene for an ultrashort optical pulse with the duration of just a few femtoseconds. For such a short pulse, the electron dynamics is coherent, and the system exhibits new features related to the topological resonance. To describe different types of the graphene-like materials, we consider the model of gapped graphene with a variable bandgap. The bandgap can be opened, for example, by applying the staggered potential, which can be realized by epitaxially growing graphene on a SiC substrate.

II. MODEL AND MAIN EQUATIONS

We consider electron dynamics in the field of the pulse with the duration of just a few femtoseconds. Taking into account that electron scattering times in graphene are of the order of or longer than 10 fs – see Refs. 32–37, we neglect the electron collisions and assume that the electron dynamics is coherent. Such dynamics is described by time-dependent Schrödinger equation (TDSE)

$$i\hbar \frac{d\Psi_{\alpha\mathbf{q}}}{dt} = H(t)\Psi_{\alpha\mathbf{q}}, \quad H(t) = H_0 - e\mathbf{F}(t)\mathbf{r}, \quad (1)$$

where $\mathbf{F}(t)$ is the electric field of the pulse, and e is electron charge. Here we assume that the electron initially (before the pulse) is in the band α ($\alpha = v$ for the valence

band (VB) and $\alpha = c$ for the conduction band (CB)) with crystal momentum \mathbf{q} .

Field-free Hamiltonian H_0 is the nearest-neighbor two-band tight binding Hamiltonian of gapped graphene^{38–40}

$$H_0 = \begin{pmatrix} \Delta_g/2 & \gamma f(\mathbf{k}) \\ \gamma f^*(\mathbf{k}) & -\Delta_g/2 \end{pmatrix}, \quad (2)$$

where Δ_g is the band gap, $\gamma = -3.03$ eV is the hopping integral, and

$$f(\mathbf{k}) = \exp\left(i\frac{ak_y}{\sqrt{3}}\right) + 2\exp\left(-i\frac{ak_y}{2\sqrt{3}}\right)\cos\left(\frac{ak_x}{2}\right), \quad (3)$$

where $a = 2.46$ Å is the lattice constant.

The energies of CB and VB can be found from Hamiltonian H_0 and are given by the following expression

$$E_\alpha(\mathbf{k}) = \pm\sqrt{\gamma^2|f(\mathbf{k})|^2 + \Delta_g^2/4}, \quad (4)$$

where signs \pm stand for CB ($\alpha = c$) and VB ($\alpha = v$), respectively.

The applied electric field generates both intraband and interband electron dynamics. The intraband dynamics is described by the Bloch acceleration theorem⁴¹, which determines the time-dependent electron wavevector, $\mathbf{k}(\mathbf{q}, t)$, as follows

$$\mathbf{k}(\mathbf{q}, t) = \mathbf{q} + \frac{e}{\hbar} \int_{-\infty}^t \mathbf{F}(t') dt', \quad (5)$$

where \mathbf{q} is the initial electron wavevector. In relation to the Bloch trajectories (5), we also define the separatrix as a set of initial points \mathbf{q} for which the electron trajectories pass precisely through the corresponding K or K' points⁴². Its parametric equation is

$$\mathbf{q}(t) = \mathbf{K} - \mathbf{k}(0, t), \quad \text{or} \quad \mathbf{q}(t) = \mathbf{K}' - \mathbf{k}(0, t), \quad (6)$$

where $t \in (-\infty, \infty)$ is a parameter.

To determine the the intraband electron dynamics, we solve TDSE in terms of the Houston functions⁴³, which are adiabatic solutions for intraband dynamics,

$$\Phi_{\alpha\mathbf{q}}^{(H)}(\mathbf{r}, t) = \Psi_{\mathbf{k}(\mathbf{q}, t)}^{(\alpha)}(\mathbf{r}) \exp\left(i\phi_\alpha^{(D)}(\mathbf{q}, t) + i\phi_\alpha^{(B)}(\mathbf{q}, t)\right), \quad (7)$$

where $\Psi_{\mathbf{k}(\mathbf{q}, t)}^{(\alpha)}$ are the Bloch functions. Here the dynamic phase, $\phi_\alpha^{(D)}$, and the geometrical phase, $\phi_\alpha^{(B)}$, are defined as

$$\phi_\alpha^{(D)}(\mathbf{q}, t) = \frac{-1}{\hbar} \int_{-\infty}^t dt' (E_\alpha[\mathbf{k}(\mathbf{q}, t')]), \quad (8)$$

$$\phi_\alpha^{(B)}(\mathbf{q}, t) = \frac{-e}{\hbar} \int_{-\infty}^t dt' \mathbf{F} \cdot (\mathcal{A}^{\alpha\alpha}[\mathbf{k}(\mathbf{q}, t')]). \quad (9)$$

In Eq. (9), $\mathcal{A}^{\alpha\alpha} = \langle \Psi_{\mathbf{q}}^{(\alpha)} | i \frac{\partial}{\partial \mathbf{q}} | \Psi_{\mathbf{q}}^{(\alpha)} \rangle$ is the intraband Berry connection for band α , which in this model can

be found analytically as

$$\mathcal{A}_x^{cc}(\mathbf{k}) = \frac{-a\gamma^2}{\gamma^2|f(\mathbf{k})|^2 + (\Delta_g/2 - E_c)^2} \sin\frac{3ak_y}{2\sqrt{3}} \sin\frac{ak_x}{2} \quad (10)$$

$$\mathcal{A}_y^{cc}(\mathbf{k}) = \frac{a\gamma^2}{\sqrt{3}(\gamma^2|f(\mathbf{k})|^2 + (\Delta_g/2 - E_c)^2)} \times \left(\cos ak_x - \cos\frac{\sqrt{3}ak_y}{2} \cos\frac{ak_x}{2} \right) \quad (11)$$

$$\mathcal{A}_x^{vv}(\mathbf{k}) = \frac{-a\gamma^2}{\gamma^2|f(\mathbf{k})|^2 + (\Delta_g/2 + E_c)^2} \sin\frac{3ak_y}{2\sqrt{3}} \sin\frac{ak_x}{2} \quad (12)$$

$$\mathcal{A}_y^{vv}(\mathbf{k}) = \frac{a\gamma^2}{\sqrt{3}(\gamma^2|f(\mathbf{k})|^2 + (\Delta_g/2 + E_c)^2)} \times \left(\cos ak_x - \cos\frac{\sqrt{3}ak_y}{2} \cos\frac{ak_x}{2} \right) \quad (13)$$

The general solution of TDSE (1) can be expanded in the basis of the Houston functions as

$$\Psi_{\mathbf{q}}(\mathbf{r}, t) = \sum_{\alpha=c_1, c_2, v} \beta_{\alpha\mathbf{q}}(t) \Phi_{\alpha\mathbf{q}}^{(H)}(\mathbf{r}, t), \quad (14)$$

where $\beta_{\alpha\mathbf{q}}$ are the expansion coefficients, which satisfy the following system of coupled differential equations

$$i\hbar \frac{\partial B_{\mathbf{q}}(t)}{\partial t} = H'(\mathbf{q}, t) B_{\mathbf{q}}(t). \quad (15)$$

Here the wave function (the vector of state) $B_{\mathbf{q}}(t)$ and Hamiltonian in the interaction representation $H'(\mathbf{q}, t)$ are defined as

$$B_{\mathbf{q}}(t) = \begin{bmatrix} \beta_{c\mathbf{q}}(t) \\ \beta_{v\mathbf{q}}(t) \end{bmatrix}, \quad (16)$$

$$H'(\mathbf{q}, t) = -e\mathbf{F}(t) \hat{\mathcal{A}}(\mathbf{q}, t), \quad (17)$$

$$\hat{\mathcal{A}}(\mathbf{q}, t) = \begin{bmatrix} 0 & \mathcal{D}^{cv}(\mathbf{q}, t) \\ \mathcal{D}^{vc}(\mathbf{q}, t) & 0 \end{bmatrix}. \quad (18)$$

The non-Abelian Berry connection matrix elements, $\mathcal{A}^{cv} = (\mathcal{A}_x^{cv}, \mathcal{A}_y^{cv})$, which are proportional to the interband dipole matrix elements, are given by the following expressions

$$\mathcal{A}_x^{cv}(\mathbf{k}) = \mathcal{N} \left(\frac{-a}{2|f(\mathbf{k})|^2} \right) \left(\sin\frac{ak_x}{2} \sin\frac{a\sqrt{3}k_y}{2} + i\frac{\Delta_g}{2E_c} \left(\cos\frac{a\sqrt{3}k_y}{2} \sin\frac{ak_x}{2} + \sin ak_x \right) \right) \quad (19)$$

$$\mathcal{A}_y^{cv}(\mathbf{k}) = \mathcal{N} \left(\frac{a}{2\sqrt{3}|f(\mathbf{k})|^2} \right) \left(-1 - \cos\frac{a\sqrt{3}k_y}{2} \cos\frac{ak_x}{2} + 2\cos^2\frac{ak_x}{2} - i\frac{3\Delta_g}{2E_c} \sin\frac{a\sqrt{3}k_y}{2} \cos\frac{ak_x}{2} \right) \quad (20)$$

where

$$\mathcal{N} = \frac{|\gamma f(\mathbf{k})|}{\sqrt{\frac{\Delta_g^2}{4} + |\gamma f(\mathbf{k})|^2}}. \quad (21)$$

In the presence of a strong field, we solve the TDSE (15) with initial conditions that the VB is initially fully occupied and the CB is completely empty. From these solutions we can find the residual CB population and find the energy absorbed by graphene monolayer. The corresponding absorbance is defined as

$$A = \frac{\int |\beta_{c\mathbf{q}}(t = \infty)|^2 E_c(\mathbf{q}) d\mathbf{q}}{2\pi^2 c \epsilon_0 \int_{-\infty}^{\infty} |\mathbf{F}|^2 dt}, \quad (22)$$

where c is speed of light in vacuum, and ϵ_0 is the dielectric permittivity of the surrounding medium.

Below we present the results for a gapped graphene monolayer for both linearly- and circularly-polarized pulses.

III. RESULTS

A. Linearly polarized ultrafast pulse

First, we consider a linearly-polarized optical pulse that consists of a single oscillation and is polarized along the x axis, $\mathbf{F}(t) = (F_x(t), 0)$. The waveform of this pulse is set as

$$F_x(t) = F_0 (1 - 2u^2) \exp(-u^2) \quad (23)$$

where F_0 is the amplitude of the pulse, and $\tau = 1$ fs is the characteristic time of the optical oscillation.

The calculated absorbance as a function of the field amplitude is shown in Fig. 1 for different values of the bandgap, Δ_g . For the pristine graphene, $\Delta_g = 0$, the absorbance takes the universal value of $\pi\alpha \approx 2.3$ percent ($\alpha = \frac{1}{137}$ is the fine structure constant) for the field amplitudes as small as 0.002 V/Å.

With increasing the field amplitude, F_0 , the absorbance decreases for small Δ_g , $\Delta_g \lesssim 1.5$ eV, and increases for large Δ_g , $\Delta_g \gtrsim 1.5$ eV. Finally, it reaches the saturated value of ≈ 1.5 percent at $F_0 \gtrsim 0.5$ V/Å – see Fig. 1(a). Visible suppression of absorbance at small Δ_g with increasing the field amplitude can be understood by looking at the CB population distribution for different field amplitudes 0.002 , 0.2 , 0.6 , and 1 V/Å – see Fig. 2, where the results are shown for pristine graphene.

The CB population distribution is determined by the properties of the interband dipole matrix element (non-Abelian Berry connection). Namely, for pristine graphene, the x component of the interband dipole matrix element has singularities at the Dirac points, K and K' , of type $q_y/(q_x^2 + q_y^2)$, where (q_x, q_y) is the wavevector defined relative to the corresponding Dirac point. Thus the interband coupling in this case is strongly localized

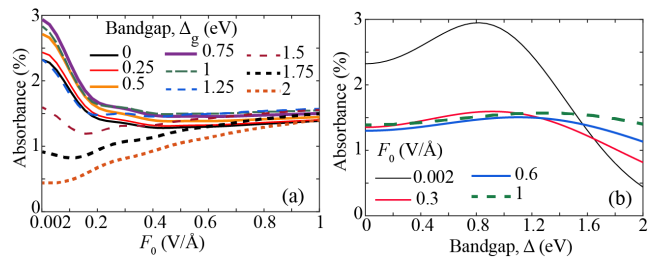


FIG. 1. (Color online) Absorbance in gapped graphene (a) as a function of the field amplitude for $\Delta_g = 0, 0.25, 0.5, 0.75, 1, 1.25, 1.5, 1.75, 2$ eV and (b) as a function of bandgap for $F_0 = 0.002, 0.3, 0.6, 1$ V/Å. The applied optical pulse is linearly polarized along x direction.

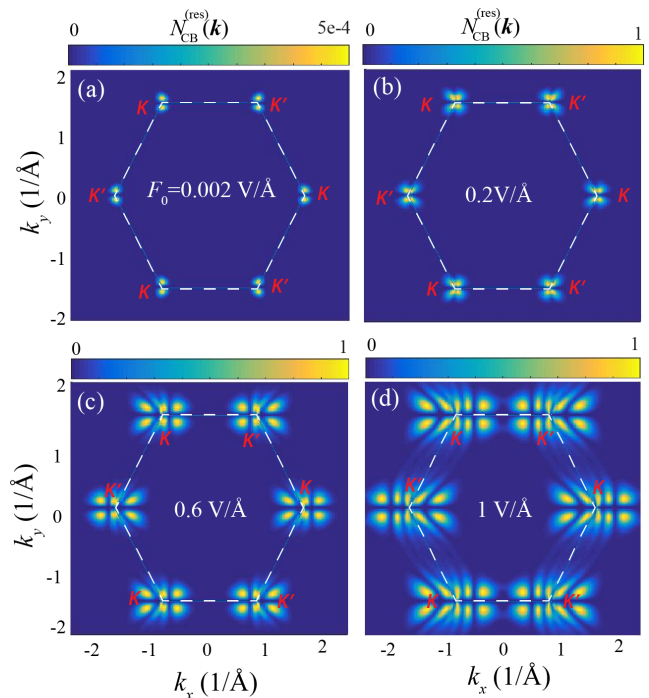


FIG. 2. (Color online) Residual CB population of graphene with $\Delta_g = 0$ induced by a linearly polarized pulse in x direction. The field amplitude is (a) 0.002 , (b) 0.2 , (c) 0.6 , and (d) 1 V/Å. The white dash line indicates the boundary of the first Brillouin zone.

at the Dirac points. As a result, if during the pulse an electron passes through the region that is very close to the Dirac point, then strongly localized interband coupling rotates the electron pseudospin by 180° . It means that if before the passage the electron is in the VB then after the passage the electron is completely transferred to the CB and vice versa. The double passage of the Dirac point leaves the electron in the original state, i.e., in the VB.

Due to this property of the interband coupling, the CB population distribution has the following structure.

For the field amplitude as small as 0.002 V/\AA , near each Dirac point, there are two hot spots [see Fig. 2 (a)], i.e., regions with large CB population, one above and another below the Dirac point. They are separated by dark regions, which, as mentioned above, are due to singularity of the dipole matrix elements at the Dirac points. With increasing the field amplitude each bright spot transforms into a set of dark and bright fringes [see Fig. 2 (b)-(d)], which are due to interference effects. The first appearance of such an interference pattern occurs at a field amplitude of $F_0^{(1)}$ that can be calculated as

$$F_0^{(1)} \approx 2 \frac{\hbar\omega^2}{ev_F}, \quad (24)$$

where ω is the characteristic carrier frequency of the pulse, and $v_F \sim ac = e^2/\hbar$ is the Fermi velocity of electrons. For $\hbar\omega \approx 1.6 \text{ eV}$, we obtain $F_0^{(1)} \approx 0.3 \text{ V/\AA}$. This is in a qualitative agreement with the calculation results illustrated in Fig. 2 (b)]. Note that the same field amplitude of $\sim F_0^{(1)}$ determines the onset of the saturation of the absorbance – cf. Fig. 1(a). Additionally, one can also evaluate the separation between the fringes in the reciprocal space, Δk , as

$$\Delta k = \frac{2\omega}{v_F}. \quad (25)$$

Note that this separation does not depend on the pulse amplitude, which defines the number of fringes estimated as $\approx F_0/F_0^{(1)}$. Estimating from Eq. (25), for $\hbar\omega = 1.6 \text{ eV}$, we obtain $\Delta k \approx 0.2 \text{ \AA}^{-1}$. This is in a good quantitative agreement with Fig. 2(c), (d).

As a function of the bandgap, Δ_g , the absorbance shows different types of behavior at small and large field amplitudes, F_0 , – see Fig. 1. At large F_0 , $F_0 \gtrsim \Delta_g/a$, where a is the lattice constant, the absorbance is almost independent of the bandgap, while at smaller F_0 the absorbance has strong nonmonotonic dependence on Δ_g – see Fig. 1(b). The origin of such a dependence can be understood from the CB population distribution, which is shown in Fig. 3 for the field amplitude of $F_0 = 0.002 \text{ V/\AA}$ and various bandgaps. For small Δ_g , the CB population has two maxima above and below the K and K' points. As mentioned above, in pristine graphene, i.e., at zero bandgap, these maxima are due to singularities of the interband dipole matrix element at the Dirac points. At a finite bandgap, the interband coupling is regular and has a single maximum at each Dirac point with the maximum value that is inversely proportional to the bandgap. As a result, with increasing the bandgap, the CB population distribution transforms from the two-maxima structure near each Dirac points into a single-maximum structure at the Dirac points, which occurs at $\Delta_g \approx 1 \text{ eV}$. In such a case, the absorbance increases with Δ_g – see Fig. 1(b). After that, when the bandgap increases further, the interband coupling at the Dirac point decreases, which suppresses both the CB population [see Fig. 3(d)] and the absorbance.

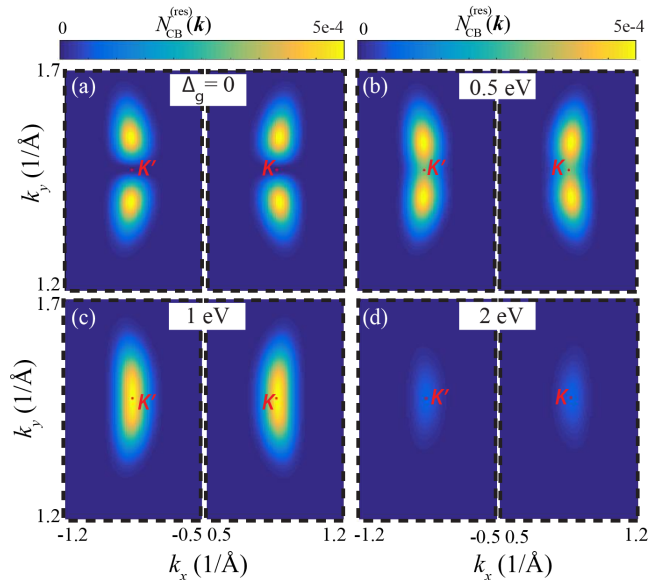


FIG. 3. (Color online) Residual CB population distribution for gapped graphene with the bandgap of $\Delta_g = 0, 0.5, 1,$ and 2 eV . The optical pulse is linearly polarized along x direction. The amplitude of the pulse is 0.002 V/\AA . The CB population distributions are shown near the K and K' points.

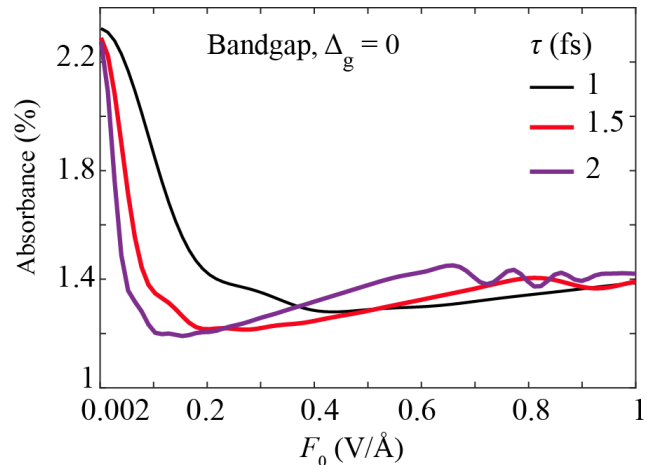


FIG. 4. (Color online) Absorbance of pristine graphene as a function of the field amplitude for different values of τ , $\tau = 1, 1.5, 2 \text{ fs}$.

Another parameter of the pulse, which determines the absorbance of the system, is the duration of the pulse, τ that determines its carrier frequency, $\omega \sim 1/\tau$. The dependence of the absorbance on τ is shown in Fig. 4 for pristine graphene with a zero bandgap. The results are shown as a function of the field amplitude. We can see from the figure that the saturated value of the absorbance, which is ≈ 1.4 percent and is achieved at large field amplitudes, does not depend on the duration of the

pulse, τ . At the same time, the field amplitude, at which the saturated value is achieved, depends on τ . Namely, with increasing τ (or, decrease of $\omega \sim 1/\tau$, the saturated value is achieved at a smaller field amplitude F_0 . We can reasonably assume that the saturation is also related to the formation of the interference fringes in the electron lattice-momentum distribution. In such a case, the field at which the saturation sets on is given by $F_0^{(1)} \propto 1/\tau^2$ – see Eq. (24). This scaling is in a reasonable agreement with the numerical results of Fig. 4.

B. Circularly polarized ultrafast pulse

Here, we consider absorption of a single-oscillation circularly-polarized pulse. The profile of the pulse, $\mathbf{F}(t) = \{F_x(t), F_y(t)\}$, is defined by the following expressions

$$F_x(t) = F_0 (1 - 2u^2) \exp(-u^2) \quad (26)$$

$$F_y(t) = 2F_0 u \exp(-u^2), \quad (27)$$

where F_0 is the amplitude of the pulse and $u = t/\tau$.

The absorbance for a circularly polarized pulse is shown in Fig. 5(a) as a function of the field amplitude, F_0 , for different bandgaps. The absorbance does not saturate at large values of F_0 , in a sharp contrast to the case of the linearly polarized pulse. At all field amplitudes the absorbance has strong dependence on the bandgap. For small Δ_g , $\Delta_g \lesssim 1.5$ eV, the absorbance first decreases with F_0 , reaches its minimum value, and then increases. For large bandgaps, $\Delta_g \gtrsim 1.5$ eV, the absorbance monotonically increases with F_0 .

The origin of nonmonotonic dependence of the absorbance at small values of Δ_g can be understood from the CB population distribution shown in Fig. 6 for pristine graphene. At small field amplitudes, $F_0 \lesssim 0.1$ V/Å, the CB population at each Dirac point, K or K' , has a single-peak structure localized at the corresponding Dirac point. Within this range of F_0 , the absorbance decreases with F_0 . Then, at $F_0 \approx 0.1$ V/Å, a single peak structure of the CB population distribution transforms into an arc that is a caustic, i.e., an image of the separatrix whose size is proportional to F_0 – see Refs. 14 and 44. With this structure of the CB population, the absorbance increases with F_0 . Finally, the absorbance reaches its maximum at $F_0 \approx 0.75$ V/Å. This is the value of F_0 at which the CB population distribution shows the first interference fringes – see Fig. 6(c). Such an interference pattern is clearly visible at large field amplitudes – see Fig. 6(d). It is due to the Bloch trajectories crossing the K, K' -valley boundaries, which is likely to limit the absorbance.

Similar to the case of a linearly polarized pulse, the absorbance for a circularly polarized pulse shows non-monotonic dependence on the bandgap at small field amplitudes – see Fig. 5(b). Namely, the absorbance first increases with Δ_g and then decreases. Such behavior is

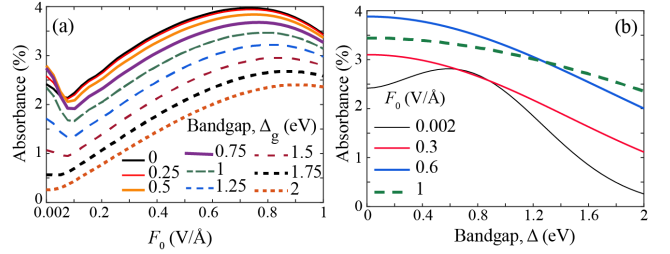


FIG. 5. (Color online) Absorbance in gapped graphene with tunable bandgap (a) as a function of the field amplitude for $\Delta_g = 0, 0.25, 0.5, 0.75, 1, 1.25, 1.5, 1.75, 2$ eV and (b) as a function of the bandgap for $F_0 = 0.002, 0.3, 0.6, 1$ V/Å. The optical pulse is circularly polarized.

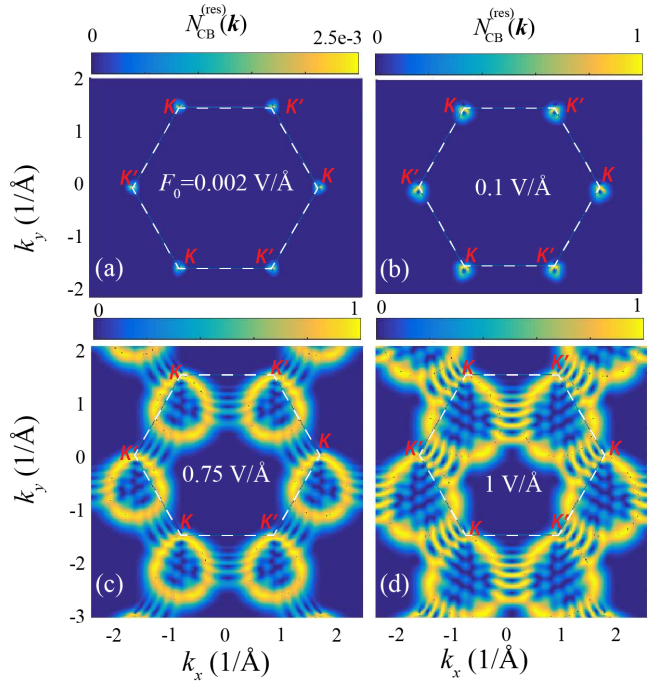


FIG. 6. (Color online) Residual CB population of graphene with $\Delta_g = 0$ induced by a circularly polarized pulse with different amplitudes 0.002, 0.1, 0.75, and 1 V/Å for panels (a)-(d), correspondingly. The white dash line indicates the boundary of the first Brillouin zone.

consistent with CB population distribution shown in Fig. 7 for the field amplitude of $F_0 = 0.002$ V/Å.

IV. CONCLUSIONS

The ultrafast absorption of optical pulses in gapped graphene is determined by specific properties of ultrafast electron dynamics, both intraband and interband, in the field of the pulse. Such dynamics strongly depends on polarization of the optical pulse, whether it is linear or

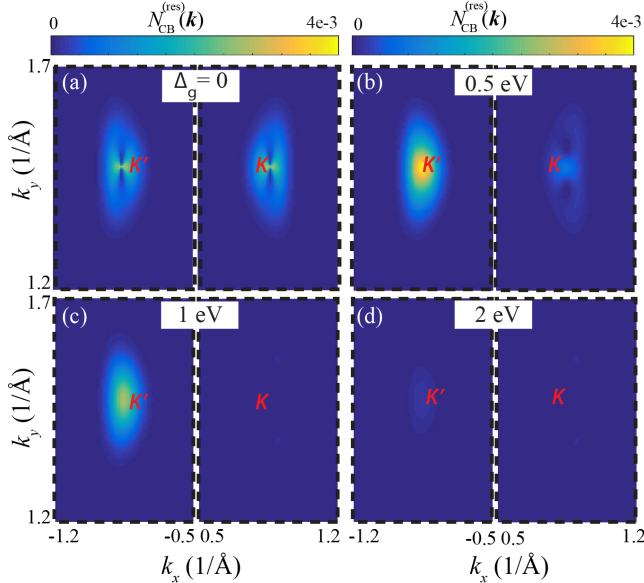


FIG. 7. (Color online) Residual CB population of gapped graphene induced by a circularly polarized pulse with the amplitude of 0.002 V/\AA . The bandgap is 0, 0.5, 1, and 2 eV, as indicated in the corresponding panels. The white dash line indicates the boundary of the first Brillouin zone.

circular. There is a fundamental difference between these two types of single-oscillation pulses. In fact, the electron Bloch trajectory in the reciprocal space passes twice through the region near the K, K' -points (where the interband coupling is large) for the linear polarization and only once for the circular polarization. As a result, the interference pattern with the dark and bright fringes is clearly visible in the CB population distribution for a linearly polarized pulse but no such interference is observed at small field amplitudes for a circularly polarized pulse in agreement with earlier results^{14,44}. Due to this effect, the absorption of the linearly- and circularly-polarized

pulses is different. Such a difference is well pronounced for relatively large field amplitudes, $F_0 \gtrsim 0.1 \text{ V/\AA}$. For small field amplitudes, the absorbance for both types of polarization behaves similarly. This is because for small field amplitudes the size of the electron displacement in the reciprocal space is less than or comparable to the size of the region with the large interband coupling. In this case, during the whole trajectory, both for linearly and circularly polarized pulses, there is a strong (or weak) interband coupling. Thus no interference pattern can be formed and no difference between the linear and circular polarizations is observed.

At large field amplitude, when the interference pattern is formed for linearly polarized pulses, the main differences between the circularly and linearly polarized pulse can be summarized as follows. While for linearly polarized pulse the absorbance as a function of the pulse amplitude is saturated at ≈ 1.4 percent, for circularly polarized pulse the absorbance does not show any saturation. The absorbance of a circularly polarized pulse can reach the value of as much as 4 percent. As a function of the bandgap, the absorbance of a linearly polarized pulse has weak dependence on Δ_g , while the absorbance of a circularly polarized pulse strongly depends on the bandgap.

ACKNOWLEDGMENTS

Major funding was provided by Grant No. DE-FG02-11ER46789 from the Materials Sciences and Engineering Division of the Office of the Basic Energy Sciences, Office of Science, U.S. Department of Energy. Numerical simulations have been performed using support by Grant No. DE-FG02-01ER15213 from the Chemical Sciences, Biosciences and Geosciences Division, Office of Basic Energy Sciences, Office of Science, US Department of Energy. The work of V.A. was supported by NSF EFRI NewLAW Grant EFMA-17 41691.

¹ A. Schiffrin, T. Paasch-Colberg, N. Karpowicz, V. Apalkov, D. Gerster, S. Muhlbrandt, M. Korbman, J. Reichert, M. Schultze, S. Holzner, J. V. Barth, R. Kienberger, R. Ernstorfer, V. S. Yakovlev, M. I. Stockman, and F. Krausz, “Optical-field-induced current in dielectrics,” *Nature* **493**, 70–74 (2012).
² V. Apalkov and M. I. Stockman, “Theory of dielectric nanofilms in strong ultrafast optical fields,” *Phys. Rev. B* **86**, 165118–1–13 (2012).
³ T. Higuchi, C. Heide, K. Ullmann, H. B. Weber, and P. Hommelhoff, “Light-field-driven currents in graphene,” *Nature* **550**, 224–228 (2017).
⁴ Elisabeth Gruber, Richard A. Wilhelm, Rmi Ptuya, Valerie Smejkal, Roland Kozubek, Anke Hierzenberger, Bernhard C. Bayer, Iigo Aldazabal, Andrey K. Kazansky, Florian Libisch, Arkady V. Krasheninnikov, Marika Schle-

berger, Stefan Facsko, Andrei G. Borisov, Andrs Arnau, and Friedrich Aumayr, “Ultrafast electronic response of graphene to a strong and localized electric field,” *Nat. Commun.* **7**, 13948 (2016).

⁵ S. A. Oliaei Motlagh, V. Apalkov, and M. I. Stockman, “Interaction of crystalline topological insulator with an ultrashort laser pulse,” *Phys. Rev. B* **95**, 085438–1–8 (2017).

⁶ S. A. O. Motlagh, J. S. Wu, V. Apalkov, and M. I. Stockman, “Fundamentally fastest optical processes at the surface of a topological insulator,” *Phys. Rev. B* **98**, 125410–1–11 (2018).

⁷ C. Heide, T. Higuchi, H. B. Weber, and P. Hommelhoff, “Coherent electron trajectory control in graphene,” *Phys. Rev. Lett.* **121**, 207401–1–5 (2018).

⁸ Christian Heide, Tobias Boolakee, Takuya Higuchi, Heiko B Weber, and Peter Hommelhoff, “Interaction of

- carrier envelope phase-stable laser pulses with graphene: the transition from the weak-field to the strong-field regime,” *New J. Phys.* **21**, 045003 (2019).
- ⁹ Dong Sun, Grant Aivazian, Aaron M. Jones, Jason S. Ross, Wang Yao, David Cobden, and Xiaodong Xu, “Ultrafast hot-carrier-dominated photocurrent in graphene,” *Nat. Nanotechnol.* **7**, 114 (2012).
 - ¹⁰ Hiroki Mashiko, Yuta Chisuga, Ikufumi Katayama, Katsuya Oguri, Hiroyuki Masuda, Jun Takeda, and Hideki Gotoh, “Multi-petahertz electron interference in cr:al2o3 solid-state material,” *Nat. Commun.* **9**, 1468 (2018).
 - ¹¹ Hee Jun Shin, Van Luan Nguyen, Seong Chu Lim, and Joo-Hiuk Son, “Ultrafast nonlinear travel of hot carriers driven by high-field terahertz pulse,” *J. Phys. B: At. Mol. Opt. Phys.* **51**, 144003 (2018).
 - ¹² Takuya Higuchi, Christian Heide, Konrad Ullmann, Heiko B. Weber, and Peter Hommelhoff, “Light-field-driven currents in graphene,” *Nature* **550**, 224–228 (2017).
 - ¹³ M. Trushin, A. Grupp, G. Soavi, A. Budweg, D. De Fazio, U. Sassi, A. Lombardo, A. C. Ferrari, W. Belzig, A. Leitenstorfer, and D. Brida, “Ultrafast pseudospin dynamics in graphene,” *Phys. Rev. B* **92**, 165429 (2015).
 - ¹⁴ S. A. Oliaei Motlagh, J.-S. Wu, V. Apalkov, and M. I. Stockman, “Femtosecond valley polarization and topological resonances in transition metal dichalcogenides,” *Phys. Rev. B* **98**, 081406(R)–1–6 (2018).
 - ¹⁵ D. Sun, J. W. Lai, J. C. Ma, Q. S. Wang, and J. Liu, “Review of ultrafast spectroscopy studies of valley carrier dynamics in two-dimensional semiconducting transition metal dichalcogenides,” *Chin. Phys. B* **26** (2017), 10.1088/1674-1056/26/3/037801.
 - ¹⁶ Jun Zhang, Hao Ouyang, Xin Zheng, Jie You, Runze Chen, Tong Zhou, Yizhen Sui, Yu Liu, Xiang’ai Cheng, and Tian Jiang, “Ultrafast saturable absorption of mos2 nanosheets under different pulse-width excitation conditions,” *Opt. Lett.* **43**, 243–246 (2018).
 - ¹⁷ Yong Sing You, Yanchun Yin, Yi Wu, Andrew Chew, Xiaoming Ren, Fengjiang Zhuang, Shima Gholam-Mirzaei, Michael Chini, Zenghu Chang, and Shambhu Ghimire, “High-harmonic generation in amorphous solids,” *Nat. Commun.* **8**, 724 (2017).
 - ¹⁸ H. Z. Liu, Y. L. Li, Y. S. You, S. Ghimire, T. F. Heinz, and D. A. Reis, “High-harmonic generation from an atomically thin semiconductor,” *Nat. Phys.* **13**, 262–266 (2017).
 - ¹⁹ A. Kaiser, B. Rethfeld, M. Vicanek, and G. Simon, “Microscopic processes in dielectrics under irradiation by subpicosecond laser pulses,” *Phys. Rev. B* **61**, 11437–11450 (2000).
 - ²⁰ H. G. Rosa, J. A. Castaneda, C. H. B. Cruz, L. A. Padilha, J. C. V. Gomes, E. A. T. de Souza, and H. L. Fragnito, “Controlled stacking of graphene monolayer saturable absorbers for ultrashort pulse generation in erbium-doped fiber lasers,” *Opt. Mater. Express* **7**, 2528–2537 (2017).
 - ²¹ S. Kumar, M. Anija, N. Kamaraju, K. S. Vasu, K. S. Subrahmanyam, A. K. Sood, and C. N. R. Rao, “Femtosecond carrier dynamics and saturable absorption in graphene suspensions,” *Appl. Phys. Lett.* **95** (2009), 10.1063/1.3264964.
 - ²² F. Gesuele, “Ultrafast hyperspectral transient absorption spectroscopy: Application to single layer graphene,” *Photonics* **6** (2019), 10.3390/photonics6030095.
 - ²³ A. K. Geim and K. S. Novoselov, “The rise of graphene,” *Nat Mater* **6**, 183–191 (2007).
 - ²⁴ A. H. Castro Neto, F. Guinea, N. M. R. Peres, K. S. Novoselov, and A. K. Geim, “The electronic properties of graphene,” *Rev. Mod. Phys.* **81**, 109–162 (2009).
 - ²⁵ S. Z. Butler, S. M. Hollen, L. Y. Cao, Y. Cui, J. A. Gupta, H. R. Gutierrez, T. F. Heinz, S. S. Hong, J. X. Huang, A. F. Ismach, E. Johnston-Halperin, M. Kuno, V. V. Plashnitsa, R. D. Robinson, R. S. Ruoff, S. Salahuddin, J. Shan, L. Shi, M. G. Spencer, M. Terrones, W. Windl, and J. E. Goldberger, “Progress, challenges, and opportunities in two-dimensional materials beyond graphene,” *Acc Nano* **7**, 2898–2926 (2013).
 - ²⁶ K. S. Novoselov, A. K. Geim, S. V. Morozov, D. Jiang, M. I. Katsnelson, I. V. Grigorieva, S. V. Dubonos, and A. A. Firsov, “Two-dimensional gas of massless Dirac fermions in graphene,” *Nature* **438**, 197–200 (2005).
 - ²⁷ A. Kormanyos, G. Burkard, M. Gmitra, J. Fabian, V. Zolyomi, N. D. Drummond, and V. Fal’ko, “k.p theory for two-dimensional transition metal dichalcogenide semiconductors (vol 2, 022001, 2015),” *2d Materials* **2** (2015).
 - ²⁸ Y. Ye, J. Xiao, H. L. Wang, Z. L. Ye, H. Y. Zhu, M. Zhao, Y. Wang, J. H. Zhao, X. B. Yin, and X. Zhang, “Electrical generation and control of the valley carriers in a monolayer transition metal dichalcogenide,” *Nat. Nanotechnol.* **11**, 598–602 (2016).
 - ²⁹ D. Jariwala, V. K. Sangwan, L. J. Lauhon, T. J. Marks, and M. C. Hersam, “Emerging device applications for semiconducting two-dimensional transition metal dichalcogenides,” *Acc Nano* **8**, 1102–1120 (2014).
 - ³⁰ S. Azar Oliaei Motlagh, Fatemeh Nematollahi, Vadym Apalkov, and Mark I. Stockman, “Topological resonance and single-optical-cycle valley polarization in gapped graphene,” *Phys. Rev. B* **100**, 115431 (2019).
 - ³¹ Seyyedeh Azar Oliaei Motlagh, Fatemeh Nematollahi, Aranyo Mitra, Ahmal Jawad Zafar, Vadym Apalkov, and Mark I Stockman, “Ultrafast optical,” *Journal of Physics: Condensed Matter* (2019), 10.1088/1361-648X/ab4fc7.
 - ³² E. H. Hwang and S. Das Sarma, “Single-particle relaxation time versus transport scattering time in a two-dimensional graphene layer,” *Phys. Rev. B* **77**, 195412–1–6 (2008).
 - ³³ M. Breusing, S. Kuehn, T. Winzer, E. Malic, F. Milde, N. Severin, J. P. Rabe, C. Ropers, A. Knorr, and T. Elsaesser, “Ultrafast nonequilibrium carrier dynamics in a single graphene layer,” *Phys. Rev. B* **83**, 153410 (2011).
 - ³⁴ Ermin Malic, Torben Winzer, Evgeny Bobkin, and Andreas Knorr, “Microscopic theory of absorption and ultrafast many-particle kinetics in graphene,” *Phys. Rev. B* **84**, 205406 (2011).
 - ³⁵ D. Brida, A. Tomadin, C. Manzoni, Y. J. Kim, A. Lombardo, S. Milana, R. R. Nair, K. S. Novoselov, A. C. Ferrari, G. Cerullo, and M. Polini, “Ultrafast collinear scattering and carrier multiplication in graphene,” *Nat Commun* **4**, 1987–1–9 (2013).
 - ³⁶ I. Gierz, J. C. Petersen, M. Mitrano, C. Cacho, I. C. Turcu, E. Springate, A. Stohr, A. Kohler, U. Starke, and A. Cavalleri, “Snapshots of non-equilibrium Dirac carrier distributions in graphene,” *Nat. Mater.* **12**, 1119–24 (2013).
 - ³⁷ Andrea Tomadin, Daniele Brida, Giulio Cerullo, Andrea C. Ferrari, and Marco Polini, “Nonequilibrium dynamics of photoexcited electrons in graphene: Collinear scattering, Auger processes, and the impact of screening,” *Phys. Rev. B* **88**, 035430 (2013).
 - ³⁸ S. Y. Zhou, G. H. Gweon, A. V. Fedorov, P. N. First, W. A. de Heer, D. H. Lee, F. Guinea, A. H. Castro Neto, and A. Lanzara, “Substrate-induced bandgap opening in epitaxial graphene,” *Nat. Mater.* **6**, 770 (2007).
 - ³⁹ Thomas G. Pedersen, Antti-Pekka Jauho, and Kjeld

- Pedersen, “Optical response and excitons in gapped graphene,” *Phys. Rev. B* **79**, 113406 (2009).
- ⁴⁰ P. K. Pyatkovskiy, “Dynamical polarization, screening, and plasmons in gapped graphene,” *J. Condens. Matter Phys.* **21**, 025506 (2008).
- ⁴¹ F. Bloch, “Über die Quantenmechanik der Elektronen in Kristallgittern,” *Z. Phys. A* **52**, 555–600 (1929).
- ⁴² H. K. Keldarsh, V. Apalkov, and M. I. Stockman, “Attosecond strong-field interferometry in graphene: Chirality, singularity, and Berry phase,” *Phys. Rev. B* **93**, 155434–1–7 (2016).
- ⁴³ W. V. Houston, “Acceleration of electrons in a crystal lattice,” *Phys. Rev.* **57**, 184–186 (1940).
- ⁴⁴ S. A. Oliaei Motlagh, F. Nematollahi, V. Apalkov, and M. I. Stockman, “Topological resonance and single-optical-cycle valley polarization in gapped graphene,” *Phys. Rev. B* **100**, 115431 (2019).